Prosaposin maintains adult neural stem cells in a state associated with deep quiescence

Miriam Labusch, Melina Thetiot, Emmanuel Than-Trong, David Morizet, Marion Coolen, Hugo Varet, Rachel Legendre, Sara Ortica, Laure Mancini, Laure Bally-Cuif

Please cite this article in press as: Labusch et al., Prosaposin maintains adult neural stem cells in a state associated with deep quiescence, Stem Cell Reports (2024), https://doi.org/10.1016/j.stemcr.2024.02.007

Stem Cell Reports
Article
ISSCR
OPEN ACCESS

Prosaposin maintains adult neural stem cells in a state associated with deep quiescence

Miriam Labusch,[1,2] Melina Thetiot,[1] Emmanuel Than-Trong,[1,4] David Morizet,[1,2] Marion Coolen,[1,5] Hugo Varet,[3] Rachel Legendre,[3] Sara Ortica,[1] Laure Mancini,[1,2,6] and Laure Bally-Cuif[1,7,*]
[1]Institut Pasteur, Université Paris Cité, CNRS UMR3738, Zebrafish Neurogenetics Unit, 75015 Paris, France
[2]Sorbonne Université, Collège doctoral, 75005 Paris, France
[3]Institut Pasteur, Université Paris Cité, Platform Biomics, 75015 Paris, France
[4]Present address: Neuroscience of Neuron, Glia, Vessel Interactions, Vision Institute, INSERM 0968, 17 rue Moreau, 75012 Paris, France
[5]Present address: Université Paris Cité, Developmental Brain Disorders Laboratory, Imagine Institute, INSERM UMR 1163, 75015 Paris, France
[6]Present address: Laboratoire Reproduction et Développement des Plantes, ENS de Lyon, Lyon, France
[7]Lead contact
*Correspondence: laure.bally-cuif@pasteur.fr
https://doi.org/10.1016/j.stemcr.2024.02.007

SUMMARY

In most vertebrates, adult neural stem cells (NSCs) continuously give rise to neurons in discrete brain regions. A critical process for maintaining NSC pools over long periods of time in the adult brain is NSC quiescence, a reversible and tightly regulated state of cell-cycle arrest. Recently, lysosomes were identified to regulate the NSC quiescence-proliferation balance. However, it remains controversial whether lysosomal activity promotes NSC proliferation or quiescence, and a finer influence of lysosomal activity on NSC quiescence duration or depth remains unexplored. Using RNA sequencing and pharmacological manipulations, we show that lysosomes are necessary for NSC quiescence maintenance. In addition, we reveal that expression of *psap*, encoding the lysosomal regulator Prosaposin, is enriched in quiescent NSCs (qNSCs) that reside upstream in the NSC lineage and display a deep/long quiescence phase in the adult zebrafish telencephalon. We show that shRNA-mediated *psap* knockdown increases the proportion of activated NSCs (aNSCs) as well as NSCs that reside in shallower quiescence states (signed by *ascl1a* and *deltaA* expression). Collectively, our results identify the lysosomal protein Psap as a (direct or indirect) quiescence regulator and unfold the interplay between lysosomal function and NSC quiescence heterogeneities.

INTRODUCTION

Adult neural stem cells (NSCs) produce neurons within discrete regions of most vertebrate brains, including the mouse subependymal zone of the lateral ventricle (SEZ), the subgranular zone of the dentate gyrus of the hippocampus (SGZ), and the zebrafish pallium (Diotel et al., 2020; Labusch et al., 2020). NSC maintenance is permitted, in part, by their residing in quiescence, a reversible and actively maintained state of cell-cycle arrest corresponding, in that case, to the G0 phase of the cell cycle (Urbán et al., 2019). A high frequency of NSC cell-cycle entry (referred to as NSC activation) is linked with NSC exhaustion (Engler et al., 2018; Imayoshi et al., 2010; Paik et al., 2009; Schäffner et al., 2018). Molecular pathways such as Notch2/3 signaling promote NSC quiescence in the different neurogenic domains, but single-cell RNA sequencing (scRNA-seq), *in vivo* functional assays (e.g., the speed of NSC reactivation upon Notch signaling blockade and intravital imaging), further show that quiescence is heterogeneous: NSCs can be found in shallower or deeper, or shorter or longer, quiescence in zebrafish (Alunni et al., 2013; Mancini et al., 2023; Morizet et al., 2023) and mouse (Dulken et al., 2017; Llorens-Bobadilla et al., 2015; Mizrak et al., 2019; Shin et al., 2015). Notably, a preactivated state was identified by the expression of *Ascl1,* encoding a basic helix-loop-helix transcription factor important for the activation of previously quiescent NSCs (Andersen et al., 2014a; Blomfield et al., 2019; Pilz et al., 2018; Urbán et al., 2016). Our recent results in the adult zebrafish pallium also highlight that the expression of *deltaA* (*deltaA*^{pos}) correlates with NSCs that on average display shorter quiescence durations than *deltaA*-negative (*deltaA*^{neg}) NSCs and are further advanced along the neurogenesis lineage (Mancini et al., 2023). Aside from these few examples, the cellular and molecular mechanisms underlying the control of quiescence depth/length remain incompletely understood.

Recently, attention has been given to differences in subcellular organelles between activated (cycling) NSCs (aNSCs) and quiescent NSCs (qNSCs). Among these, lysosomes emerged as novel regulators of NSC quiescence. Work in mice showed that qNSCs are enriched in lysosomes compared to aNSCs in the SGZ and SEZ (Kobayashi et al., 2019; Leeman et al., 2018). However, these studies show discrepant results upon lysosomal perturbation. Impairment of lysosome activity through pharmacological inhibition of the vacuolar H(+)-ATPase with bafilomycin A (BafA) leads to decreased activation of qNSCs in response to growth factors in the SEZ due to accumulations of protein aggregates (Leeman et al., 2018). In contrast, in the SGZ, BafA treatment leads to the accumulation of activated epidermal growth factor receptor (EGFR), Notch1, and

Please cite this article in press as: Labusch et al., Prosaposin maintains adult neural stem cells in a state associated with deep quiescence, Stem Cell Reports (2024), https://doi.org/10.1016/j.stemcr.2024.02.007

the Notch1 intracellular domain (NICD), increasing NSC activation (Kobayashi et al., 2019). Whether these differences are due to the different neurogenic niches or to different experimental designs remains undeciphered. Furthermore, next to their role in proteostasis maintenance, lysosomes act as important players in nutrient and pathogen sensing, as well as membrane repair (Mony et al., 2016), and it remains to be studied whether the effect of lysosome perturbation on quiescence also involves these pathways. Finally, it is unknown whether lysosomal activity relates to quiescence heterogeneities between NSCs.

To address these issues, we focused on NSCs of the zebrafish adult pallium, which are easily accessible for transient functional manipulations *in vivo*, and for which we generated a comprehensive scRNA-seq database and *in situ* readouts identifying qNSC heterogeneities correlating with differences in quiescence depth or length (Mancini et al., 2023; Morizet et al., 2023). We report here that lysosomal activity is necessary for NSC quiescence in this system, and we identify the lysosomal protein Prosaposin (Psap) as a critical player in this activity. First, *psap* expression is highest in *deltaA*^{neg} qNSCs, which display deepest/longest quiescence. Second, *psap* knockdown promotes qNSCs transition through the *deltaA*^{pos} state of shallower/shorter quiescence and NSC activation. These results reinforce the view that lysosomal activity promotes NSC quiescence and further highlight Psap as a likely player in this process.

RESULTS

Lysosomes are necessary for NSC quiescence

Adult pallial NSCs in zebrafish and mice are radial glial cells expressing glial fibrillary acidic protein (GFAP) (Ganz et al., 2010; März et al., 2010). Transgenic reporter lines for *gfap* but also for the progenitor gene *her4.3* characterize the same population of progenitors in the adult zebrafish brain (Than-Trong et al., 2020). At any given time, only ~5%–10% of NSCs are expressing the cell-cycle markers proliferating cell nuclear antigen (PCNA) or minichromosome maintenance protein 2 (MCM2), and are therefore defined as activated (Dray et al., 2021). By exclusion, other NSCs are considered quiescent. Because NSCs in different (sub)states are intermingled *in situ*, combined markers are needed to distinguish between aNSCs (*gfap*^{pos} or *her4*^{pos}, Pcna^{pos}), pre-activated qNSCs (*gfap*^{pos} or *her4*^{pos}, Pcna^{neg}, *ascl1a*^{pos}), and, among other qNSCs, those in shallow/shorter quiescence (*deltaA*^{pos} qNSCs: *gfap*^{pos} or *her4*^{pos}, Pcna^{neg}, *deltaA*^{pos}) and those in deep/longer quiescence (*deltaA*^{neg} qNSCs: *gfap*^{pos} or *her4*^{pos}, Pcna^{neg}, *ascl1a*^{neg}, *deltaA*^{neg}). *deltaA:gfp* is also expressed in nonstem neural progenitors (NPs) (equivalent to mammalian transit amplifying progenitors), which are *gfap*^{neg} and *her4*^{neg}. When the *deltaA:gfp* marker is used in the absence of NSC markers such as *gfap* or *her4*, it cannot distinguish between NSCs and NPs, and we therefore refer to *deltaA*^{pos} cells as "progenitors" (Figure 1A).

To identify pathways regulating NSC quiescence, with a possible link to quiescence depth, we used double transgenic Tg(*her4:drfp);* Tg(*mcm5:gfp*) fish and two paradigms predicted to highlight deep vs. shallower quiescence. First, in adult fish (3 months postfertilization [MPF]), we performed bulk RNA-seq on fluorescence-activated cell sorting (FACS)-sorted RFP^{high}, GFP^{neg} qNSCs and RFP^{pos}, GFP^{pos} aNSCs. *her4.3* (Figure S1A; see (Morizet et al., 2023) is a target of Notch signaling, which promotes quiescence (Alunni et al., 2013; Dray et al., 2021). We identified 3,048 genes upregulated in RFP^{high} qNSCs and 1,890 genes upregulated in aNSCs (Tables S1 and S2). As expected for aNSCs, gene set enrichment analysis confirmed the enrichment for KEGG (Kyoto Encyclopedia of Genes and Genomes) gene sets associated with cell division, which include cell cycle (Figure S1B) and DNA replication (Figure S1C), as well as ribosomal activity (Figure S1D), because aNSCs exhibit higher protein synthesis than qNSCs (Llorens-Bobadilla et al., 2015). Focusing on proteostasis, we observed enrichment of the proteasomal pathway in aNSCs (Figure S1E) and enrichment of the lysosomal pathway (Figure S1F) and the lysosome-related pathways autophagy (Figure S1G) and endocytosis (Figure S1H) in RFP^{high} qNSCs. When operating Gene Ontology (GO) analysis, we identified the KEGG lysosomal pathway as highly enriched in RFP^{high} qNSCs (Figure 1B). Then, we also generated a dataset in which we compared the bulk transcriptome of qNSCs between 1.5- and 3.5-MPF fish, stages between which deeper quiescence is progressively instated (Tables S3 and S4). GO analysis identified the KEGG lysosomal pathway as significantly enriched at 3.5 MPF (Figure 1C), pointing to a pathway that becomes more prominent with time, as previously suggested between adult and aged mice (Leeman et al., 2018).

Together, these data suggest that qNSCs may harbor more lysosomes than aNSCs, or increased lysosomal activity, or both. To address this, we performed flow cytometry analysis of freshly dissociated lysotracker-stained cells from adult pallia dissected from double transgenic Tg(*gfap:egfp);* Tg(*mcm5:nls-rfp*) fish, allowing us to dissociate between GFP^{pos}; RFP^{neg} qNSCs and GFP^{pos}; RFP^{pos} aNSCs (Figure S2A). Lysotracker probes are fluorophores linked to a weak base that is only partially protonated at neutral pH and will emit fluorescence in acidic compartments, and therefore in lysosomes (Chikte et al., 2014). We detected a decrease to 61.34% (median; interquartile range [IQR] 60.70%–61.99%) in the normalized mean intensity of lysotracker fluorescence in aNSCs compared to qNSCs (Figure 1D), suggesting that qNSCs harbor more or enlarged lysosomes. Whole-mount immunohistochemistry (IHC)

Please cite this article in press as: Labusch et al., Prosaposin maintains adult neural stem cells in a state associated with deep quiescence, Stem Cell Reports (2024), https://doi.org/10.1016/j.stemcr.2024.02.007

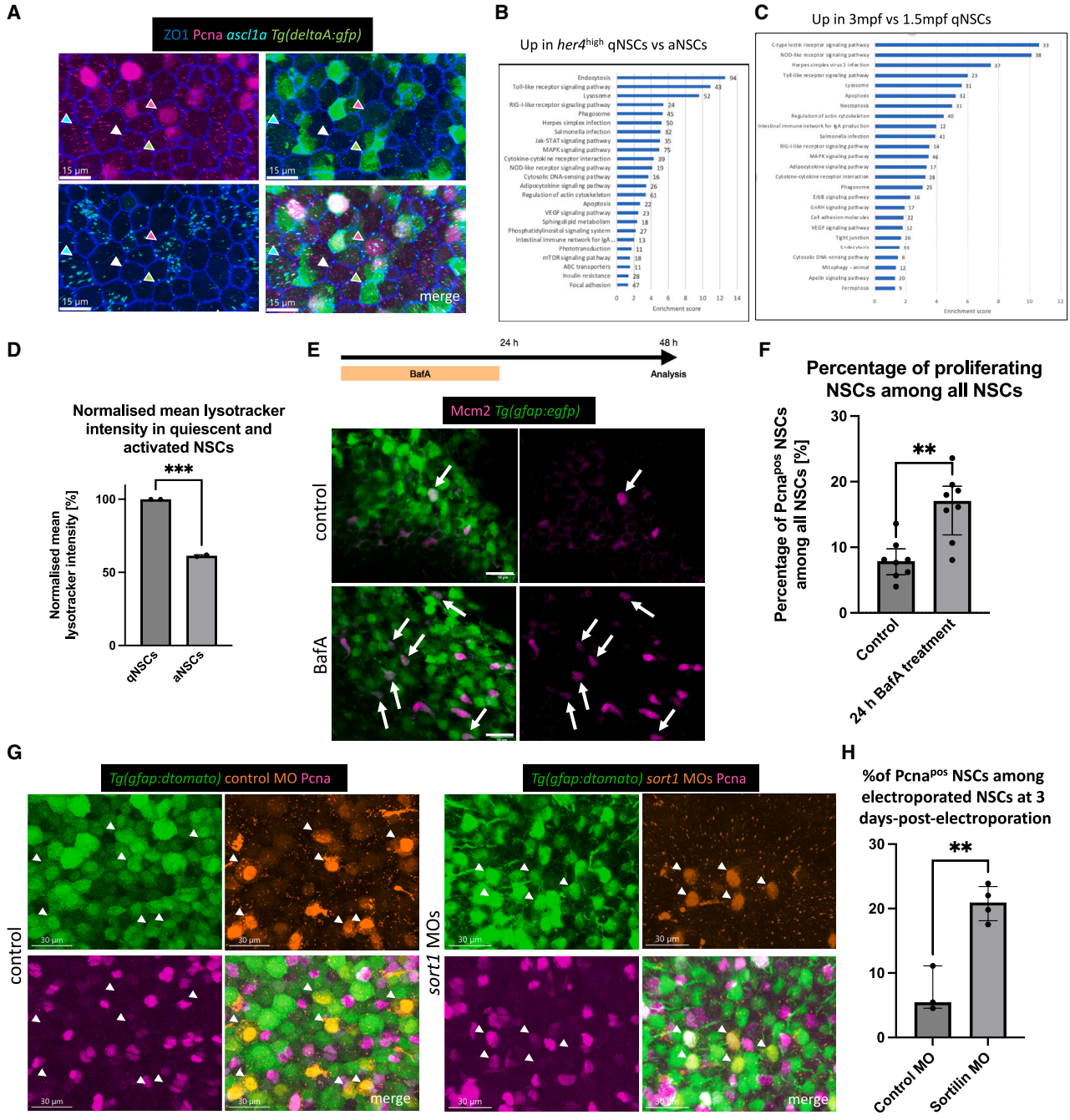

Figure 1. Lysosomes are involved in adult neural stem cell quiescence

(A) Whole-mount immunostaining for ZO1 (tight junctions, blue), PCNA (proliferation, magenta), and GFP (transcriptional reporter for *deltaA*, green), with RNAScope against *ascl1a* transcripts (preactivation, cyan). Dorsal "apical" view of the pallial ventricular zone at 3 MPF. Green arrow: *deltaA*^{pos} quiescent progenitors, white arrow: *deltaA*^{neg} qNSC, cyan: pre-activated progenitors, magenta: activated progenitors. Scale bar: 15 µm.

(B) KEGG pathways enriched in qNSCs vs. aNSCs based on GO analysis of the RNA-seq data (RFP^{high}, GFP^{neg} vs. RFP^{pos}, GFP^{pos} cells from 3 MPF Tg(*gfap:egfp*); Tg(*mcm5:nls-rfp*) fish). x axis: enrichment score; numbers next to the bars: number of genes included in this pathway.

(C) KEGG pathways enriched in qNSCs at 3.5 months vs. qNSCs at 1.5 months based on GO of the RNA-seq data. As in (B).

(D) Normalized mean LysoTracker intensity (bar plot with SD; each dot is 1 independent experiment with 10 pooled brains). Unpaired t test, ***p = 0.0003.

(legend continued on next page)

Please cite this article in press as: Labusch et al., Prosaposin maintains adult neural stem cells in a state associated with deep quiescence, Stem Cell Reports (2024), https://doi.org/10.1016/j.stemcr.2024.02.007

for the lysosomal protein Lamp1 and the proliferation marker PCNA was performed in parallel on transgenic Tg(*gfap:egfp*) fish to detect lysosomes in qNSCs and aNSCs *in situ*, and a representative image is provided in Figure S2B. We next wondered whether these lysosomes may be involved in quiescence maintenance. To impair lysosomal activity, we incubated organotypic slices of adult Tg(*gfap:egfp*) zebrafish pallia in 20 nM BafA for 24 h followed by 24 h of recovery (Figure 1E). Quantifying Pcna^{pos} GFP^{pos} aNSCs vs. Pcna^{neg} GFP^{pos} qNSCs revealed a significant percentual increase of aNSCs upon BafA treatment vs. control treatment (median and IQR: control 7.89%, 5.81%–9.76% vs. BafA treated 17.06%, 11.90%–19.32%) (Figure 1F). We verified that the BafA treatment itself did not cause toxicity (Figure S2C). Overall, we conclude that lysosomal content is enriched in the quiescent vs. activated NSC states and that lysosomal activity is critically involved in the maintenance of quiescence.

Next, to better understand whether quiescence control involves the proteostasis activity of lysosomes (Mony et al., 2016), we focused on Sortilin1, a sorting receptor of the vacuolar protein sorting 10 family that facilitates lysosome-mediated protein degradation. Sortilin1 is ubiquitously expressed in many tissues but is most abundant in the CNS (Andersen et al., 2014b). The zebrafish duplicates *sort1a* and *sort1b* were expressed together at a high level in qNSCs in our bulk dataset, and were also detectable in our scNSC dataset of the adult zebrafish pallium (Morizet et al., 2023) (Figures S2D and S2E). To knock down Sort1 function, we used previously validated splice-morpholino oligonucleotides (MOs) directed against *sort1a* and *sort1b* (De Muynck et al., 2013), which we electroporated *in vivo* into adult NSCs in Tg(*gfap:dTomato*) adult fish following intracerebral injection. We found that abrogating Sort1 function led to a significant increase in the proportion of aNSCs among cells electroporated with *sort1a*/*sort1b* MOs compared to control MOs (median and IQR: control 5.45%, 4.55%–11.11% vs. *sort1a*/*sort1b* MOs 20.93%, 18.11%–23.42%) (Figures 1G and 1H), reaching levels very similar to those obtained upon BafA treatment. Overall, we conclude that lysosomes are enriched in qNSCs that exhibit deep/long quiescence, and that their proteostasis activity promotes NSC quiescence in the adult brain *in vivo*.

Psap is heterogeneously expressed in NSCs during their quiescence phase

To further challenge whether NSC quiescence involves proteolysis control by lysosomes, as proposed (Kobayashi et al., 2019; Leeman et al., 2018), and to unravel through which molecular players, we analyzed the expression of the genes that contributed to the enrichment of the lysosomal pathway in qNSCs in our RNA-seq datasets. This led us to select *psap*, a gene encoding a glycoprotein involved in the activation of hydrolases in the lysosomes (Kishimoto et al., 1992), and to date, solely implicated in lysosomal proteostasis. In addition, cells deficient for Sort1 exhibit impaired trafficking of Psap to the lysosomes and enhanced release of Psap into the extracellular medium (Aguilera et al., 2023; Hassan et al., 2004; Lefrancois et al., 2003; Zeng et al., 2009). We found that *psap* was expressed at levels 3.5 times higher in qNSCs vs. aNSCs in a reproducible manner (Figure 2A). It is also enriched 2.3 times in 3- compared to 1.5-MPF qNSCs (Table S3). RNAScope *in situ* hybridization (ISH) experiments for *psap* further revealed heterogeneous expression levels among NSCs (Figure 2B). Finally, and more important, *psap* transcript levels in individual qNSCs in our scRNA-seq dataset were stronger in cells transcriptionally distant from *pcna*-expressing aNSCs, *ascl1a*^{pos} preactivated qNSCs, and *deltaA*-expressing NSCs (Figures 2C and S3A–S3C).

To assess the relationship between *psap*, the number of lysosomes, and qNSC states associated with different quiescence depth/length, we first tested whether *deltaA* expression already correlates with distinct metabolic states signed by NSCs harboring more or fewer lysosomes. We used double transgenic Tg(*gfap:dtomato*); Tg(*deltaA:egfp*) fish, allowing us to dissociate dTomato^{pos}, GFP^{pos} *deltaA*^{pos} NSCs, and dTomato^{pos} GFP^{neg} *deltaA*^{neg} NSCs for flow cytometry analysis after lysotracker staining (Figure S3D). When analyzing the mean intensity of lysotracker fluorescence, we confirmed that *deltaA*^{pos} NSCs contain fewer lysosomes than *deltaA*^{neg} NSCs (median and IQR: 54.93%, 48.17%–61.69% in *deltaA*^{pos} NSCs) (Figure 2D). We therefore analyzed *psap* expression in regard to *deltaA* in NSCs by combining immunostainings for ZO1 (tight junctions), dTomato, and GFP in double transgenic Tg(*gfap:dTomato*); Tg(*deltaA:egfp*) fish with RNAScope for *psap* (Figure 2E).

(E) Experimental design and view of telencephalic organotypic slices after IHC for GFP (NSCs, green) and MCM2 (proliferation, magenta) after control and BafA treatment. Arrows: Mcm2^{pos},GFP^{pos} NSCs. Scale bars: 10 μm.

(F) Proportion of proliferating NSCs (Pcna^{pos}) among all NSCs. Each dot represents 1 animal (with 1–4 treated slices per animal). Bar at median with IQR. Mann-Whitney test, **p = 0.0026.

(G) Whole-mount IHC for Tg*(gfap:dTomato)* (NSCs, green), and PCNA (proliferation, magenta) in combination with control and *sort1a/sort1b*-MO-electroporated cells (orange). Dorsal view of the pallial ventricular zone at 3 MPF. Arrows point to electroporated NSCs. Scale bar: 30 μm.

(H) Percentage of activated NSCs among all electroporated NSCs 3 days after control- and *sort1*-MO electroporation. Each dot is 1 fish. Line at median with IQR. Unpaired t test with Welch's correction, **p = 0.0064.

Please cite this article in press as: Labusch et al., Prosaposin maintains adult neural stem cells in a state associated with deep quiescence, Stem Cell Reports (2024), https://doi.org/10.1016/j.stemcr.2024.02.007

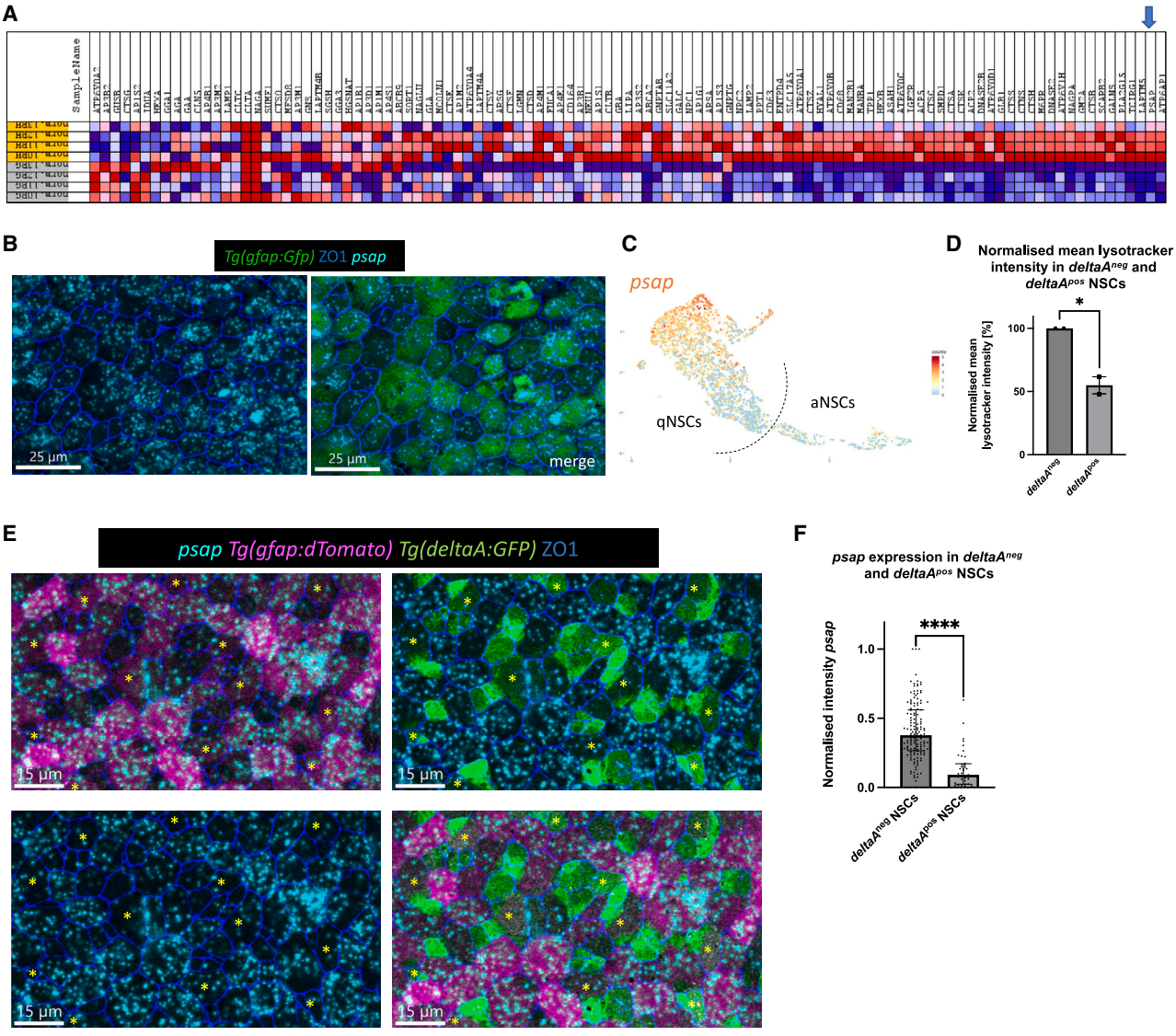

Figure 2. *Psap* is heterogeneously expressed in quiescent NSCs

(A) Gene expression heatmap of the lysosome KEGG gene set (red = upregulated, blue = downregulated). Each line is 1 biological replicate (gray = aNSCs, yellow = deeply qNSCs – *her4*^{high}), based on our bulk RNA-seq dataset. Arrow to *psap*.

(B) Whole-mount RNAScope for *psap* (cyan) and IHC for *Tg(gfap:eGFP)* (NSCs, green) and ZO1 (tight junctions, blue). Dorsal view of the pallial ventricular zone at 3 MPF. *Psap* is heterogeneously expressed. Scale bar: 25 µm.

(C) Uniform manifold approximation and projection of *psap* expression in NSCs (scRNA-seq dataset of Morizet et al., 2023). *Psap* is enriched in cells with deepest/longest quiescence (compare with Figure S4A).

(D) Normalized mean LysoTracker intensity in *deltaA*^{pos} and *deltaA*^{neg} NSCs; bar plot with SD. Each dot is 1 independent experiment with 10 pooled brains. Unpaired t test, *p = 0.0218.

(E) Whole-mount RNAScope for *psap* (cyan) and triple IHC for *Tg(gfap:dTomato)* (magenta), *Tg(deltaA:eGFP)* (green), and ZO1 (tight junctions, blue). Dorsal view of the pallial ventricular zone at 3 MPF; merged channel, bottom right. Yellow asterisks indicate examples of *deltaA*^{pos} NSCs. Scale bars: 15 µm.

(F) Normalized intensity sum of *psap* after two-dimensional projection in *deltaA*^{neg} and *deltaA*^{pos} cells within the *gfap:dTomato*^{pos} NSC population. The highest intensity value has been set to 1. Every dot represents 1 cell; 3 independent experiments. Mann-Whitney test, ****p $\leq$ 0.0001.

We found that *psap* expression was significantly higher in *deltaA*^{neg} (median and IQR: 0.38, 0.26%–0.56%) compared to *deltaA*^{pos} (median and IQR: 0.09, 0.02%–0.17%) NSCs (Figure 2F). These results point to increased *psap* expression in qNSCs with deep/long quiescence, as opposed to qNSCs with shallower/shorter quiescence.

Psap maintains NSCs in a state of deep quiescence

To explore the function of *psap* in quiescence *in vivo*, we chose a mosaic loss-of-function approach to focus on cell-autonomous effects. Due to the duration of quiescence in adult pallial NSCs (doubling times on average of 124 days for *deltaA*^{neg} and 28 days for *deltaA*^{pos} NSCs) (Mancini et al., 2023), we needed a method that could conditionally abrogate Psap function over several days/weeks while allowing cell tracking. Thus, we adapted and validated for the adult brain a recent RNAi knockdown method allowing long-term chase and concomitant tracing (Giacomotto et al., 2015). We designed nine shRNAs targeting the endogenous *psap* transcript and three control shRNAs and cloned them in 3′ of pCMV (porcine cytomegalovirus):*h2amCherry*. Following electroporation into adult NSCs *in vivo*, we first verified that pCMV:*h2amCherry-RNAi(psap)* NSCs had a strong reduction of *psap* transcript levels compared to surrounding nonelectroporated cells at 3 and 14 days post-electroporation (dpe), as measured using RNAscope (median and IQR: for 3 days control 114.2%, 113.0%–115.4% vs. RNAi(*psap*) 24.92%, 13.73%–28.62%; for 14 days control 137.9%, 130.4%–145.3% vs. RNAi(*psap*) 32.59%, 21.07%–40.00%) (Figures S4A–S4D). Decreased expression of *psap* did not lead to significant changes in lysosome number and volume after 5 days, as measured *in situ* using Lamp1 immunostaining (median and IQR: for lysosome number: control 94.10%, 94.02%–94.19% vs. RNAi(*psap*) 92.27%, 82.84%–101.70%; for lysosomal volume: control 89.13%, 65.50%–112.80% vs. RNAi(*psap*) 106.10%, 99.05%–121.50%) (Figures S4E and S4F). We then proceeded to use this construct for loss-of-function experiments and electroporated Tg(*gfap:egfp*) fish to analyze H2amCherry^{pos}, GFP^{pos} NSCs at 3, 5, and 14 days after knockdown (Figures 3A and 3B). Activation events were quantified by equaling each Pcna^{pos} doublet (sister cells postdivision) and each Pcna^{pos} singlet to one event. We observed a significantly increased proportion of H2amCherry^{pos}, GFP^{pos}, Pcna^{pos} aNSC events at 5 dpe upon *psap* knockdown. At 3 and 14 dpe we observed a trend increase (median and IQR: 3 days, control 0.00%, 0.00%–1.61% vs. RNAi(*psap*) 7.47%, 2.28%–12.49%; 5 days control 1.67%, 0.00%–1.98% vs. RNAi(*psap*) 10.53%, 6.85%–12.77%; 14 days control 1.25%, 0.38%–3.89% vs. RNAi(*psap*) 5.46%, 3.27%–8.27%) (Figures 3C–3E). We conclude that *psap* knockdown increases NSC entry into the cell cycle. Monitoring the ratio of Pcna^{pos} doublets over singlets further indicated that the cell cycle per se was not visibly affected (median and IQR: 3 days, control 0.0%, 0.0%–0.0%, vs. RNAi(*psap*) 11.61%, 0.25%–30.56%; 5 days control 0.00%, 0.00%–33.33% vs. RNAi(*psap*) 20.00%, 5.57%–33.33%) (Figures S4G and S4H). Hence, loss-of-function experiments of *psap* increase NSC proliferation *in vivo*, identifying Psap as a novel factor necessary for NSC quiescence.

Increased NSC activation upon Psap abrogation is, in part, associated with a progression along the NSC lineage hierarchy

Quiescence depth/duration, the successive steps from quiescence to activation, and NSC lineage progression are intertwined processes on which Psap could act, with a common output measured by Pcna expression. For example, the duration of the *ascl1a*^{pos} preactivation state could be modified. In addition, NSC quiescence and fate dynamics vary along lineage progression: self-renewing *deltaA*^{neg} NSCs in deep/long quiescence generate, upon division, *deltaA*^{pos} NSCs of shallow/short quiescence, characterized by stochastic fates biased toward the generation of neurons (Mancini et al., 2023; Than-Trong et al., 2020). Thus, the increased NSC proliferation observed upon Psap abrogation can be interpreted as a general release of quiescence, a shortened preactivation phase, a progression along the lineage, or combinations of these events.

To address this issue, we monitored the expression of *ascl1a* and *deltaA* upon loss of Psap function. Using RNAscope to quantify *ascl1a* expression at the single-cell level *in situ* in Tg(*gfap:egfp*) fish to identify NSCs (Figure 4A), we observed a significant increase in the proportion of GFP^{pos}, *ascl1a*^{pos} NSCs 5 days post-*psap* knockdown (median and IQR: control 9.41%, 8.00%–10.82% vs. RNAi (*psap*) 25.00%, 19.27%–36.94%) (Figure 4B), indicating a shift toward the preactivated and/or committed state.

Next, we knocked down *psap* in Tg(*deltaA:egfp*) fish and monitored *deltaA* expression in electroporated cells. As suggested by the shift in state demonstrated by *ascl1a* expression, we observed an increase in the proportion of H2amCherry^{pos}, GFP^{pos} cells at 5 dpe upon RNAi, from 22.97%, 21.43%–27.88% (control RNAi, median and IQR) to 42.35%, 37.82%–51.71% (*psap* RNAi, median and IQR) (Figures 4C and 4D). However, despite the increased number of proliferating cells induced by *psap* RNAi (median and IQR: control 5.26%, 2.58%–6.58% vs. RNAi(*psap*) 9.73%, 6.75%–14.35%) (Figure 4E), the proportion of proliferating cells among *deltaA*^{pos} progenitors remained constant (median and IQR: control 16.67%, 6.92%–25.00% vs. RNAi(*psap*) 21.86%, 11.07%–25.89%) (Figure 4F). A similar conclusion was reached regarding the proportion of proliferating cells among *deltaA*^{neg} progenitors, although the low proliferation rate of *deltaA*^{neg} NSCs makes this analysis

Please cite this article in press as: Labusch et al., Prosaposin maintains adult neural stem cells in a state associated with deep quiescence, Stem Cell Reports (2024), https://doi.org/10.1016/j.stemcr.2024.02.007

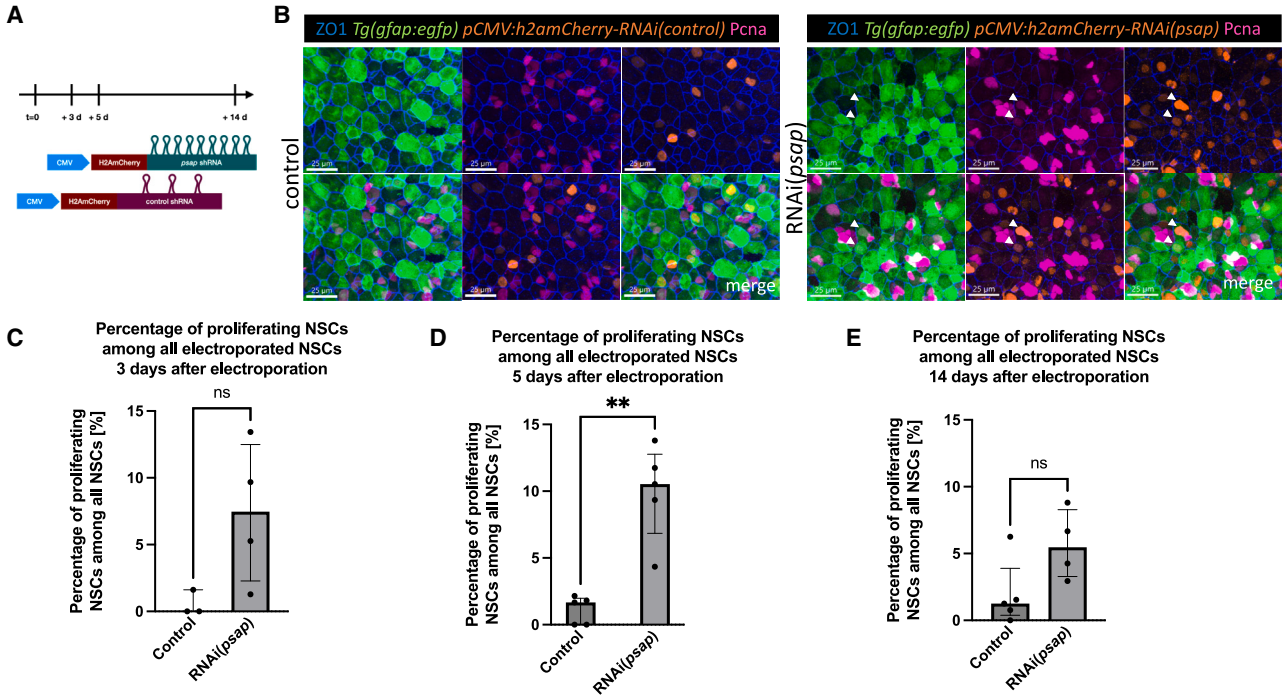

Figure 3. *Psap* activity promotes NSC quiescence

(A) Experimental design: at day 0, *pCMV:RNAi(psap)* and *pCMV:RNAi(control)* were electroporated in pallial NSCs in 3 MPF fish. The fish were sacrificed at 3, 5, and 14 dpe.

(B) Whole-mount IHC for ZO1 (tight junctions, blue), GFP (NSCs, green), H2amCherry (electroporated cells, orange), and PCNA (proliferation, magenta) at 5 dpe in RNAi control and RNAi(*psap*) electroporated fish. Dorsal view of the pallium. Scale bar: 25 μm. Arrows: proliferating NSCs.

(C) Percentage of aNSCs among all electroporated NSCs at 3 dpe in control vs. *psap*-RNAi. Each dot is 1 fish. Line at median with IQR. Mann-Whitney test, ns, not significant, p = 0.1143.

(D) Percentage of aNSCs among all electroporated NSCs at 5 dpe in control vs. *psap*-RNAi. Each dot is 1 fish. Line at median with IQR. Mann-Whitney test, **p = 0.0079.

(E) Percentage of activated NSCs among all electroporated NSCs at 14 dpe in control vs. *psap*-RNAi. Each dot is 1 fish. Line at median with IQR. Mann-Whitney test, p = 0.0635.

difficult (median and IQR: control 0.00%, 0.00%–0.00% vs. RNAi(*psap*) 0.00%, 0.00%–1.28%) (Figure 4G). Together, these observations suggest that loss of *psap* leads to an initial shift toward the *deltaA*^{pos} state, within which the transition toward activation and/or the proliferative behavior is not changed per se.

Neuronal generation is preserved upon Psap abrogation

Finally, we aimed to address whether the fate of NSCs is altered after the loss of *psap*. We first analyzed the fate of sister cells upon *psap* knockdown relative to *deltaA* expression: *deltaA*^{neg} NSCs systematically self-renew upon division, whereas *deltaA*^{pos} NSCs progressively engage toward neurogenesis, identifying different stemness potential (Mancini et al., 2023). Control and RNAi(*psap*) were electroporated into Tg(*deltaA:egfp*) fish, and the relative distribution of division modes in doublets of sister cells was analyzed at 5 dpe. These distributions did not appear statistically different between control and RNAi(*psap*) electroporated cells (median and IQR: Mann-Whitney tests, *deltaA*^{neg}/*deltaA*^{neg} doublets: control: 0.00%, 0.00%–0.00%, RNAi(*psap*): 6.25%, 0.00%–27.38%, p = 0.3929; *deltaA*^{neg}/*deltaA*^{pos} doublets: control: 33.33%, 0.00%–100.00%, RNAi (*psap*): 33.93%, 0.00%–70.00%, p = 0.9524; *deltaA*^{pos}/*deltaA*^{pos} doublets: control: 66.67%, 0.00%–100.00%, RNAi (*psap*): 41.43%, 25.00%–71.88%, p = 0.6905).

To further substantiate this result, we analyzed the generation of more committed cell fates by focusing on terminal NSC divisions generating NPs (Gfap^{neg}). For this, electroporations of RNAi(*psap*) into the Tg(*gfap:egfp*) line were used and NSC/NSC, NSC/NP, and NP/NP doublets were counted. At 3, 5, and 14 dpe, we found that the relative distribution of NSC division modes was also similar between control

Please cite this article in press as: Labusch et al., Prosaposin maintains adult neural stem cells in a state associated with deep quiescence, Stem Cell Reports (2024), https://doi.org/10.1016/j.stemcr.2024.02.007

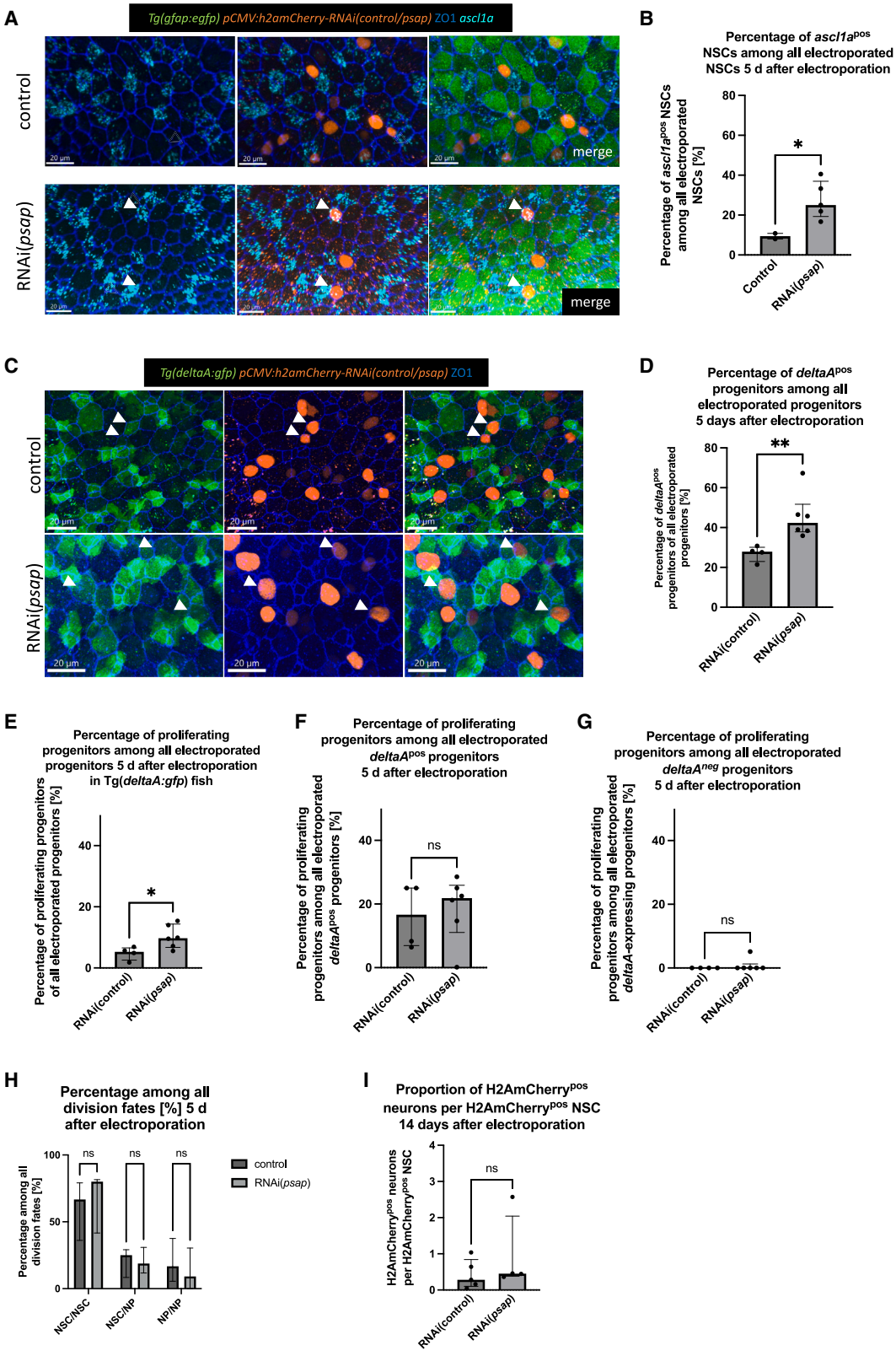

(legend on next page)

Please cite this article in press as: Labusch et al., Prosaposin maintains adult neural stem cells in a state associated with deep quiescence, Stem Cell Reports (2024), https://doi.org/10.1016/j.stemcr.2024.02.007

and RNAi(*psap*) electroporated cells (at 5 dpe, median and IQR: Mann-Whitney tests, NSC/NSC doublets: control: 66.67%, 8.33%–29.17%, RNAi(*psap*): 80.00%, 41.67%–81.53%, p = 0.3929; NSC/NP doublets: control: 25.00%, 0.00%–100.00%, RNAi(*psap*): 18.75%, 11.69%–30.83%, p = 0.9524; NP/NP doublets: control: 16.67%, 5.55%–37.5%, RNAi(*psap*): 9.091%, 0.00%–30.36%, p = 0.6905) (Figure 4H) (see also Figure S4I for 3 dpe and S4J 14 dpe). Finally, we counted H2amCherry^{pos} cells at 14 dpe and calculated the ratio of neurons per NSC. We did observe large variations across samples in both control and *psap* RNAi samples and no significant difference between the control and knockdown conditions overall (median and IQR: control 0.2813%, 0.1032%–0.8405% vs. RNAi(*psap*) 0.4518%, 0.3831%–2.043%) (Figure 4I).

DISCUSSION

This work brings novel molecular insight into the control of NSC quiescence in the adult brain. We show that lysosomal activity in adult zebrafish pallial NSCs correlates with and is needed for their quiescence. *In vivo*, we further show that, like lysosomal inhibition, blocking the sorting receptor Sortilin induces NSC proliferation. Finally, we provide evidence for the functional necessity of Psap to maintain an NSC state associated with deep quiescence. These results together add support to the fact that lysosomes are positive regulators of NSC quiescence, likely through their role in autophagy, and show that proteins such as Psap further refine this control to include the regulation of quiescent NSC substates associated with different quiescence depth or duration.

At the technical level, we made use of RNAi, a technique long debated in the zebrafish field due to nonspecific defects and high toxicity in embryos, likely due to a highjacking of the microRNA machinery (Zhao et al., 2008). In 2015, efficient downregulation of mRNA through shRNAs was reported (Giacomotto et al., 2015). Adapting the system to single NSCs was successful in terms of knockdown efficiency, but it also did not show any signs of toxicity, as assessed by NSC morphology and survival. The long-term perdurance of the induced knockdown with this system (at least up to 14 days), compared to morpholinos (3–4 days) (Katz et al., 2016), is advantageous, and it will be interesting to see whether other adult tissues are good targets for this method.

We show that qNSCs of the adult zebrafish pallium harbor more lysosomes and display a transcriptome enriched for genes associated with the endosomal-lysosomal compartment compared to their activated counterparts. Accordingly, the impairment of lysosomal function leads to an increase in NSC proliferation, which aligns with findings in the mouse SGZ (Kobayashi et al., 2019) but not the SEZ (Leeman et al., 2018). Possible reasons for discrepancies between these mouse studies include their different neurogenic niches and experimental setups. The zebrafish adult pallial germinal niche appears, for its anterior component (Da-Dm, the focus of our *in situ* analyses), ontogenetically and molecularly related to the dorsal wall of the SEZ, itself closer to the SGZ in terms of marker expression (e.g., *Hopx*) (Zweifel et al., 2018), later entry into quiescence during development (Berg et al., 2019) and increased NSC quiescence depth (Marcy et al., 2023; Zweifel et al., 2018), and cortical origin. The zebrafish adult pallial germinal niche also joins and includes the hippocampal area more posterolaterally. As in Kobayashi et al. (2019), we found that concentrations of BafA at 50 nM led to toxicity. Lysosomal blockade can also drive cells into senescence (Kang et al., 2011), and it remains

Figure 4. *Psap* knockdown increases the proportion of NSCs in states associated with shallow quiescence, without affecting neurogenesis output

(A) RNAScope for *ascl1a* (turquoise) and whole-mount IHC for *gfap*:GFP (green), H2amCherry (electroporated cells, orange), and ZO1 (tight junctions, blue) 5 days after electroporation of control (top) and *psap*-RNAi (bottom) construct in Tg(*gfap:egfp*) fish. Dorsal view of the pallial ventricular zone at 3 MPF. Arrows: examples of *ascl1a*^{pos} cells. Scale bar: 20 μm.

(B) Percentage of *ascl1a*^{pos} NSCs among all electroporated NSCs 5 days after control and *psap*-RNAi. Line at median with IQR. Unpaired t test with Welch's correction, *p = 0.0112.

(C) Whole-mount IHC for *gfap*:GFP (green), H2amCherry (electroporated cells, orange), and ZO1 (tight junctions, blue) 5 days after electroporation of RNAi control (top) and RNAi(*psap*) construct. Dorsal view of the pallium at 3 MPF. Arrows: GFP^{pos} progenitor cells. Scale bar: 20 μm.

(D) Percentage of *deltaA*^{pos} progenitor cells among all electroporated progenitor cells 5 days after control and *psap*-RNAi electroporation. Each dot is 1 fish. Line at median with IQR. Mann-Whitney test, **p = 0.0095.

(E–G) Percentage of proliferating progenitors 5 days after control and *psap*-RNAi electroporation among all of the electroporated progenitors (E), among all of the electroporated *deltaA*^{pos} progenitors (F), and among all of the electroporated *deltaA*^{neg} progenitors (G). Each dot represents 1 animal. Line at median with IQR. Mann-Whitney tests: (E) *p = 0.0381, (F) p = 0.9286, and (G) p > 0.9999.

(H) Percentage of the different division modes in control vs. RNAi(*psap*) electroporated cells at 5 dpe (see Figure S4 for 3 and 14 dpe). x axis: state of the 2 sister cells in doublets. Lines at median with IQR. Mann-Whitney tests, NSC/NSC doublets: p = 0.8413; NSC/NP doublets: p = 0.7936; NP/NP doublets: p = 0.6429.

(I) Ratio of neurons relative to NSCs in electroporated cells and their progeny. Each dot is 1 fish. Line at median with IQR. Mann-Whitney test, p = 0.4127.

to be functionally tested whether any of these experimental setups increase senescence.

We further demonstrate that *psap* is highly expressed in deeply quiescent NSCs. Psap is a prominent lysosomal protein (under its cleaved forms, saposins, which hydrolyze sphingolipids) but it can also be secreted, to boost lysosomal function in receiving cells (Zhou et al., 2017) and/or act as a neurotrophic factor (Meyer et al., 2014). To center on the lysosomal function of Psap, we focused on the cell-autonomous effects of *psap* manipulations. Specifically, the knockdown of *psap* shifted NSCs toward substates associated with shallower quiescence (as defined by *deltaA* and *ascl1a*) and with activation. We note that not all NSCs responded to manipulations of Psap or lysosomal activity. This is in agreement with the fact that not all NSCs express *psap*, but they may also reflect windows of responsiveness to Psap or lysosomal activity within the deep quiescence state. The fact that lysosomal activity can modulate quiescence depth is an idea that was postulated in embryonic fibroblasts (Fujimaki et al., 2019) and is compatible with several studies in hematopoietic stem cells (García-Prat et al., 2021; Liang et al., 2020). Although this was not directly addressed for NSCs, preexisting studies highlighting progressive changes in NSC states are in line with our conclusion. For example, in cultured NSCs from the hippocampus, mRNA levels for the transcription factor EB or cathepsins increase progressively during the first 3 days of incubation with the quiescence inducer bone morphogenetic protein. Conversely, BafA leads to progressive increases in activated EGFR and Notch1-ICD, which is compatible with a transition from quiescence to activation through shallower quiescence stages (Kobayashi et al., 2019).

Under physiological conditions, changes in NSC quiescence duration in the adult zebrafish pallium and mouse SGZ are concomitant with NSC progression toward a neurogenic fate (Bottes et al., 2021; Mancini et al., 2023; Than-Trong et al., 2020). Thus, a limitation to current studies, including ours, is to distinguish between a bona fide function of lysosomal factors (e.g., Psap) in quiescence depth/duration per se vs. in NSC position along the lineage (i.e., self-renewal vs. an engagement toward a neurogenic fate). A primary effect on quiescence could secondarily affect neurogenesis commitment, and a primary effect on neurogenesis commitment could secondarily affect quiescence. In the future, it will be important to resolve whether *deltaA* and *ascl1a* expression induced under *psap* knockdown reflect decreased quiescence depth, increased commitment, or both. Verifying this point will require more extensive lineage tracing because the number of RNAi (*psap*) NSCs in electroporation experiments is unfortunately too low for these cells to be profiled and their state characterized in depth.

A remaining question will be to identify the relevant targets of Psap. In the adult mouse SGZ, impaired lysosomal function leads to the accumulation of phosphorylated EGFR, Notch1-ICD, and Cyclin D1 (Kobayashi et al., 2019). Our attempts to detect such changes in adult zebrafish pallial NSCs *in vivo* (using anti-EGFR IHC and a direct Notch3 signaling reporter) remained unsuccessful. We also were technically limited *in vivo* to address the hydrolysis of sphingolipids (Kishimoto et al., 1992) or related changes in metabolism due to defective mitochondria and oxidative phosphorylation (Arora et al., 1997; Kogot-Levin and Saada, 2014). Mitochondrial function depends on intact lysosomes (García-Prat et al., 2021; Ho et al., 2017; Liang et al., 2020) and is important for hippocampal neurogenesis (Beckervordersandforth et al., 2017). Thus, future directions could explore the link between lysosomes and mitochondria in NSCs.

EXPERIMENTAL PROCEDURES

Resource availability

Lead contact

laure.bally-cuif@pasteur.fr.

Materials availability

All of the materials generated in this work are available upon request.

Data and code availability

This work uses two RNA-seq datasets.

- The bulk RNA-seq dataset was generated in this study. The accession number for the raw data reported in this paper is GEO: GSE239598 (https://www.ncbi.nlm.nih.gov/geo/query/acc.cgi?acc=GSE239598).
- The scRNA-seq dataset was generated by Morizet et al. (2023). The manuscript is available at doi: https://doi.org/10.1101/2023.02.27.530203), and its raw data are available on GEO: GSE225863 (https://www.ncbi.nlm.nih.gov/geo/query/acc.cgi?acc=GSE225863.

Animals

The *Tg(mcm5:nls-rfp)*^{ip} transgenic line generated for this study, as well as wild-type (AB) and other transgenic zebrafish lines (see supplemental experimental procedures), were maintained using standard protocols. Three-to 4-month-old adult fish were used for analysis, unless otherwise stated. Zebrafish were kept in 3.5-L tanks at a maximal density of 5/L, in 28.5°C and pH 7.4 water. The animal study protocol was approved by the Ethics Committee no. 39 of Institut Pasteur (authorization 36936, April 26, 2022) and DDPP-2021-021 of the Direction Départementale de la Protection des Populations de Paris.

Ventricular microinjections and electroporations

See the supplemental experimental procedures.

RNAScope (ACD, Multiplex kit) whole-mount ISHs

Whole brains were fixed overnight in 4% paraformaldehyde (PFA) in PBS and kept in 100% methanol at −20°C. Following rehydration, a pigment removal solution was applied for 10 min under light to bleach the brains. Following washes, the brains were kept in Probe Diluent at 40°C and then incubated with the probe (1:50) overnight at 40°C. On day 2, the probe was rinsed at room temperature (RT), followed by 30 min Amp1 incubation at 40°C, then washes followed by 30 min Amp2 incubation at 40°C, washes, 30 min Amp3 incubation at 40°C, and washes at RT. The brains were incubated at 40°C for 15 min with horseradish peroxidase (HRP), then washed at least 6 times. Afterward, the brains were incubated for 10 min at 40°C in Tyramide Signal Amplification (TSA) solution and finally incubated with Opal 650 (1:150 in TSA) for 30 min at 40°C. The solution was washed off. Then, the brains were incubated for 15 min in an HRP blocker at 40°C.

To quantify expression of *psap* (for Figure 2F), we performed Z MaxProjection in ImageJ and then defined regions of interest based on the ZO1 signal. The number of projected slices (0.5 μm each) varied between 3 and 6 between brains (where we found visible ZO1 staining). We extracted the intensity sum for the channel in which *psap* transcripts were stained in each cell. To compare different brains, the highest value was set to 1 and the lowest to 0 for normalization. We counted at least 100 cells per brain in 3 brains. To quantify expression of *ascl1a* (for Figure 4B) in individual NSCs, we manually counted, using Imaris (Bitplane) in 3D, the fluorescent dots found in close proximity (<1 μm) to the cell nuclei, labeled with H2amCherry. We considered that a cell was *ascl1a*^{pos} when at least two dots were visible.

RNAi

We isolated the *psap* 3′ UTR by 3′ rapid amplification of cDNA end -PCR (Frohman, 1993). To design shRNAs, the miR designer (Thermo Fisher) was used, and the resulting shRNAs were ordered as double-stranded DNA (dsDNA) blocks containing surrounding regions with restriction sites matched to the final plasmid, R73. The dsDNA blocks were subcloned in TOPO TA (Strataclone), digested with XhoI and BamHI, and added to a p3 entry plasmid (R73), which can be used for cloning with the Gateway system and contained the sequence of an intron. R73 was cut with BglII and XhoI, which ensures that previously added shRNAs are not cut out of R73 but that multiple shRNAs can be added step by step at each round of cloning, in which shRNAs are chained. For *psap*, 9 shRNAs were chained. Our control construct contained 3 shRNAs. (Geneblocks: see supplemental experimental procedures.)

To validate knockdowns (Figures S4B and S4D), we used RNAScope for *psap* and quantified the RNA signal in transfected cells. We performed Z MaxProjection in ImageJ and then defined regions of interest using the ZO1 signal. The number of projected slices (0.5 μm each) varied between 9 and 23 between brains, to optimize imaging conditions depending on signal-to-noise ratio and on the curvature of the ventricular pallial surface. To neutralize the effect of these variations, each transfected cell was compared to its neighbors in the same brain. Per transfected cell, we selected four nonelectroporated neighboring cells. We then divided the average signal in electroporated cells by the average signal in non-electroporated cells to measure expression changes. These ratios were then compared between brains electroporated with the *psap* knockdown versus control constructs.

Organotypic slices generation and BafA treatment

Zebrafish brains 3 MPF were dissected in DMEM/F-12 with GlutaMax (11514436, Thermo Fisher Scientific), complemented with penicillin-streptomycin (100 IU/mL, 15140122, Thermo Fisher Scientific). Telencephala were cut into 200-μm coronal slices using a McIlwain tissue chopper or a vibratome, and the slices were placed on Millicell membranes (3–4 slices per membrane, 0.4 μm Millicell, Merck Millipore). Slices were cultured in DMEM/F-12 with GlutaMax, B-27 supplement (2%, 17504044, Thermo Fisher Scientific), N2 supplement (1%, 17502048, Thermo Fisher Scientific), insulin solution human (4 μg/mL, I9278, Sigma), D-glucose (0.3%; G8769, Sigma), amphotericin B (0.10 μg/mL, 15290026, Thermo Fisher Scientific), and penicillin-streptomycin (100 IU/mL, 15140122, Thermo Fisher Scientific), and supplemented with EGF (20 ng/mL, E4643, Sigma) and FGF2 (20 ng/mL, 100-18b, Tebu-bio). Cultures were maintained at 28.5°C under 5% CO_2 perfusion. To chemically block the vacuolar ATPase, slices were incubated for 1 day *in vitro* in either BafA (24 h, 20 nM, SML1661, Sigma-Aldrich) or DMSO (24 h, 0.02%, D8418, Sigma-Aldrich) added to the fresh culture medium. The slices were fixed 24 h posttreatment in 4% PFA for 30 min at RT and washed with PBT (PBS + 0.1% Tween-20), 3 times for 10 min, and then processed for IHC.

Quantification of lysosomes in NSCs

To generate the data for Figure 1D, dissected pallia (experiment: 10 pallia; controls: 5 pallia each) were pooled in PBS, incubated into prewarmed FACSmax solution (AMS.T200100, Amsbio) for 4 min at 28.5°C, then gently passed through a 40-μm nylon cell strainer (BD Falcon) with a 1-mL syringe plunger. The dissociated cell solution was recovered into a Petri dish and transferred to a 15-mL Falcon tube. The strainer and Petri dish were washed with FACSmax solution to increase the number of recovered cells, which were also added to the Falcon and mixed by gentle pipetting. Dissociated tissues from adult brains were centrifuged at 500 × *g* for 5 min. After discarding the supernatant, cells were incubated in a LysoTracker solution (LysoTracker, L12492, Deep Red, excitation and emission maximum: 647/668, Invitrogen, 1:10,000 in PBS) for 4 min at 28.5°C, then centrifuged at 500 × *g* for 3 min. The supernatant was discarded, and the cells were washed with PBS, centrifuged for 3 min at 500 × *g*, and finally recovered in PBS + 1 mM EDTA + 1 μg/mL DAPI. DAPI was used to remove dying cells from the analysis. Flow cytometry was performed using the Becton Dickinson FACSymphony A5. As controls, every fluorophore was measured by itself (AB with DAPI, Tg(*gfap:egfp);* Tg(*mcm5:nls-RFP*), AB with LysoTracker) through flow cytometry. A minimum of 8 × 10^5 events was recorded. To generate data for Figure 2D, a similar procedure was used starting from Tg(*gfap:dTomato);* Tg(*deltaA:eGFP*) double transgenic brains.

To generate the data for Figures S4E and S4F, we quantified the volume and number of lysosomes in electroporated cells using Imaris. To attribute lysosomes to specific cells in ventricular

progenitors that are tightly packed and of varied morphologies, we focused on an ~5-μm-thick ventricular layer (~ 1/3 of the cells' soma along the z axis) and assimilated lateral cell borders to the ZO1 staining. We then used a mask on Lamp1 in Imaris to collect information about each lysosome (intensity—mean and sum—and volume). Subsequently, data from individual cells within each brain sample were aggregated to create summary statistics for that brain; the average values for electroporated cells were normalized by the nonelectroporated surrounding cells and are represented as a percentage (100%, meaning no difference in electroporated and nonelectroporated progenitors).

Bulk transcriptomic analysis of telencephalic NSCs

See supplemental experimental procedures.

Morpholinos

See supplemental experimental procedures.

Whole-mount IHC and antibodies

See supplemental experimental procedures.

Imaging and cell counting

Images were taken using Zeiss LSM700 and LSM710 confocal microscopes using the 40× (oil) objectives. Images were processed using ZEN (Zeiss) and Imaris (Bitplane) software. Cell counts on zebrafish brains were carried out on whole-mount pallia. For electroporations, we only counted brains that had at least 30 successfully transfected NSCs. Imaris was used for all counts.

Statistical analysis

Statistical analysis was carried out for all quantitative experiments using Prism and InVivoStat (Clark et al., 2012). The normality of the residuals of the responses was assessed using normality probability plots. When data displayed an approximately Gaussian distribution, parametric tests were performed. We did not assume equal SDs, and therefore turned to t tests with Welch's corrections. The exceptions are the LysoTracker experiments, where we normalized the data and therefore expected similar SDs in biological replicates. For data that did not display a Gaussian distribution, we turned to nonparametric Mann-Whitney tests. Experimental data are expressed as median ± IQR.

SUPPLEMENTAL INFORMATION

Supplemental information can be found online at https://doi.org/10.1016/j.stemcr.2024.02.007.

ACKNOWLEDGMENTS

We are greatly indebted to Jean Giacomotto and Alisha Tromp for their help with the RNAi protocol and for providing the 3′ entry backbone for these constructs. We thank Sébastien Bedu and Nicolas Dray for help in generating the Tg(*mcm5:nls-rfp*) line. We thank the ZEN team and Thomas Wollert for input, and the Institut Pasteur CB UTechS service platform for expert assistance with the FACS analysis. This research was funded by the ANR (Labex Revive), La Ligue Nationale contre le Cancer (LNCC EL2019 BALLY-CUIF), the Fondation pour la Recherche Médicale (EQU 202203014636), the European Research Council (ERC SyG 101071786 – PEPS), CNRS, and Institut Pasteur.

AUTHOR CONTRIBUTIONS

Conceptualization, M.L. and L.B.-C.; methodology, M.L., M.T., E.T-T., S.O., L.M.; validation, M.L.; investigation, M.L.; resources, D.M., M.C., H.V., and R.L.; data curation, M.L. and E.T.-T.; writing – original draft, M.L.; writing – review & editing, all authors.; visualization, M.L.; supervision, L.B.-C.; project administration, L.B.-C.; funding acquisition, L.B.-C. All of the authors have read and agreed to the published version of the manuscript.

DECLARATION OF INTERESTS

The authors declare no competing interests.

Received: August 12, 2023
Revised: February 23, 2024
Accepted: February 26, 2024
Published: March 21, 2024

REFERENCES

Aguilera, A.C., Leiva, N., Alvarez, P.A., Pulcini, G., Pereyra, L.L., Morales, C.R., Sosa, M.Á., and Carvelli, L. (2023). Sortilin knockdown alters the expression and distribution of cathepsin D and prosaposin and up-regulates the cation-dependent mannose-6-phosphate receptor in rat epididymal cells. Sci. Rep. *13*, 3461. https://doi.org/10.1038/s41598-023-29157-z.

Alunni, A., Krecsmarik, M., Bosco, A., Galant, S., Pan, L., Moens, C.B., and Bally-Cuif, L. (2013). Notch3 signaling gates cell cycle entry and limits neural stem cell amplification in the adult pallium. Development *140*, 3335–3347. https://doi.org/10.1242/dev.095018.

Andersen, J., Urbán, N., Achimastou, A., Ito, A., Simic, M., Ullom, K., Martynoga, B., Lebel, M., Göritz, C., Frisén, J., et al. (2014a). A Transcriptional Mechanism Integrating Inputs from Extracellular Signals to Activate Hippocampal Stem Cells. Neuron *83*, 1085–1097. https://doi.org/10.1016/j.neuron.2014.08.004.

Andersen, J.L., Schrøder, T.J., Christensen, S., Strandbygård, D., Pallesen, L.T., García-Alai, M.M., Lindberg, S., Langgård, M., Eskildsen, J.C., David, L., et al. (2014b). Identification of the first small-molecule ligand of the neuronal receptor sortilin and structure determination of the receptor–ligand complex. Acta Crystallogr. D Biol. Crystallogr. *70*, 451–460. https://doi.org/10.1107/S1399004713030149.

Arora, A.S., Jones, B.J., Patel, T.C., Bronk, S.F., and Gores, G.J. (1997). Ceramide induces hepatocyte cell death through disruption of mitochondrial function in the rat. Hepatology *25*, 958–963. https://doi.org/10.1002/hep.510250428.

Beckervordersandforth, R., Ebert, B., Schäffner, I., Moss, J., Fiebig, C., Shin, J., Moore, D.L., Ghosh, L., Trinchero, M.F., Stockburger, C., et al. (2017). Role of Mitochondrial Metabolism in the Control of Early Lineage Progression and Aging Phenotypes in Adult

Hippocampal Neurogenesis. Neuron *93*, 560–573.e6. https://doi.org/10.1016/j.neuron.2016.12.017.

Berg, D.A., Su, Y., Jimenez-Cyrus, D., Patel, A., Huang, N., Morizet, D., Lee, S., Shah, R., Ringeling, F.R., Jain, R., et al. (2019). A Common Embryonic Origin of Stem Cells Drives Developmental and Adult Neurogenesis. Cell *177*, 654–668.e15. https://doi.org/10.1016/j.cell.2019.02.010.

Blomfield, I.M., Rocamonde, B., Masdeu, M.D.M., Mulugeta, E., Vaga, S., van den Berg, D.L., Huillard, E., Guillemot, F., Urbán, N., and Urbán, N. (2019). Id4 promotes the elimination of the pro-activation factor Ascl1 to maintain quiescence of adult hippocampal stem cells. Elife *8*, e48561. https://doi.org/10.7554/eLife.48561.

Bottes, S., Jaeger, B.N., Pilz, G.-A., Jörg, D.J., Cole, J.D., Kruse, M., Harris, L., Korobeynyk, V.I., Mallona, I., Helmchen, F., et al. (2021). Long-term self-renewing stem cells in the adult mouse hippocampus identified by intravital imaging. Nat. Neurosci. *24*, 225–233. https://doi.org/10.1038/s41593-020-00759-4.

Chikte, S., Panchal, N., and Warnes, G. (2014). Use of LysoTracker dyes: a flow cytometric study of autophagy. Cytometry A. *85*, 169–178. https://doi.org/10.1002/cyto.a.22312.

Clark, R.A., Shoaib, M., Hewitt, K.N., Stanford, S.C., and Bate, S.T. (2012). A comparison of InVivoStat with other statistical software packages for analysis of data generated from animal experiments. J. Psychopharmacol. *26*, 1136–1142. https://doi.org/10.1177/0269881111420313.

De Muynck, L., Herdewyn, S., Beel, S., Scheveneels, W., Van Den Bosch, L., Robberecht, W., and Van Damme, P. (2013). The neurotrophic properties of progranulin depend on the granulin E domain but do not require sortilin binding. Neurobiol. Aging *34*, 2541–2547. https://doi.org/10.1016/j.neurobiolaging.2013.04.022.

Diotel, N., Lübke, L., Strähle, U., and Rastegar, S. (2020). Common and Distinct Features of Adult Neurogenesis and Regeneration in the Telencephalon of Zebrafish and Mammals. Front. Neurosci. *14*, 568930. https://doi.org/10.3389/fnins.2020.568930.

Dray, N., Mancini, L., Binshtok, U., Cheysson, F., Supatto, W., Mahou, P., Bedu, S., Ortica, S., Than-Trong, E., Krecsmarik, M., et al. (2021). Dynamic spatiotemporal coordination of neural stem cell fate decisions occurs through local feedback in the adult vertebrate brain. Cell Stem Cell *28*, 1457–1472.e12. https://doi.org/10.1016/j.stem.2021.03.014.

Dulken, B.W., Leeman, D.S., Boutet, S.C., Hebestreit, K., and Brunet, A. (2017). Single cell transcriptomic analysis defines heterogeneity and transcriptional dynamics in the adult neural stem cell lineage. Cell Rep. *18*, 777–790. https://doi.org/10.1016/j.celrep.2016.12.060.

Engler, A., Rolando, C., Giachino, C., Saotome, I., Erni, A., Brien, C., Zhang, R., Zimber-Strobl, U., Radtke, F., Artavanis-Tsakonas, S., et al. (2018). Notch2 Signaling Maintains NSC Quiescence in the Murine Ventricular-Subventricular Zone. Cell Rep. *22*, 992–1002. https://doi.org/10.1016/j.celrep.2017.12.094.

Frohman, M.A. (1993). Rapid amplification of complementary DNA ends for generation of full-length complementary DNAs: thermal RACE. Methods Enzymol. *218*, 340–356. https://doi.org/10.1016/0076-6879(93)18026-9.

Fujimaki, K., Li, R., Chen, H., Della Croce, K., Zhang, H.H., Xing, J., Bai, F., and Yao, G. (2019). Graded regulation of cellular quiescence depth between proliferation and senescence by a lysosomal dimmer switch. Proc. Natl. Acad. Sci. USA *116*, 22624–22634. https://doi.org/10.1073/pnas.1915905116.

Ganz, J., Kaslin, J., Hochmann, S., Freudenreich, D., and Brand, M. (2010). Heterogeneity and Fgf dependence of adult neural progenitors in the zebrafish telencephalon. Glia *58*, 1345–1363. https://doi.org/10.1002/glia.21012.

García-Prat, L., Kaufmann, K.B., Schneiter, F., Voisin, V., Murison, A., Chen, J., Chan-Seng-Yue, M., Gan, O.I., McLeod, J.L., Smith, S.A., et al. (2021). TFEB-mediated endolysosomal activity controls human hematopoietic stem cell fate. Cell Stem Cell *28*, 1838–1850.e10. https://doi.org/10.1016/j.stem.2021.07.003.

Giacomotto, J., Rinkwitz, S., and Becker, T.S. (2015). Effective heritable gene knockdown in zebrafish using synthetic microRNAs. Nat. Commun. *6*, 7378. https://doi.org/10.1038/ncomms8378.

Hassan, A.J., Zeng, J., Ni, X., and Morales, C.R. (2004). The trafficking of prosaposin (SGP-1) and GM2AP to the lysosomes of TM4 sertoli cells is mediated by sortilin and monomeric adaptor proteins. Mol. Reprod. Dev. *68*, 476–483. https://doi.org/10.1002/mrd.20096.

Ho, T.T., Warr, M.R., Adelman, E.R., Lansinger, O.M., Flach, J., Verovskaya, E.V., Figueroa, M.E., and Passegué, E. (2017). Autophagy maintains the metabolism and function of young and old stem cells. Nature *543*, 205–210. https://doi.org/10.1038/nature21388.

Imayoshi, I., Sakamoto, M., Yamaguchi, M., Mori, K., and Kageyama, R. (2010). Essential roles of Notch signaling in maintenance of neural stem cells in developing and adult brains. J. Neurosci. *30*, 3489–3498. https://doi.org/10.1523/JNEUROSCI.4987-09.2010.

Kang, H.T., Lee, K.B., Kim, S.Y., Choi, H.R., and Park, S.C. (2011). Autophagy Impairment Induces Premature Senescence in Primary Human Fibroblasts. PLoS One *6*, e23367. https://doi.org/10.1371/journal.pone.0023367.

Katz, S., Cussigh, D., Urbán, N., Blomfield, I., Guillemot, F., Bally-Cuif, L., and Coolen, M. (2016). A Nuclear Role for miR-9 and Argonaute Proteins in Balancing Quiescent and Activated Neural Stem Cell States. Cell Rep. *17*, 1383–1398. https://doi.org/10.1016/j.celrep.2016.09.088.

Kishimoto, Y., Hiraiwa, M., and O'Brien, J. (1992). Saposins: structure, function, distribution, and molecular genetics. J. Lipid Res. *33*, 1255–1267. https://doi.org/10.1016/S0022-2275(20)40540-1.

Kobayashi, T., Piao, W., Takamura, T., Kori, H., Miyachi, H., Kitano, S., Iwamoto, Y., Yamada, M., Imayoshi, I., Shioda, S., et al. (2019). Enhanced lysosomal degradation maintains the quiescent state of neural stem cells. Nat. Commun. *10*, 5446. https://doi.org/10.1038/s41467-019-13203-4.

Kogot-Levin, A., and Saada, A. (2014). Ceramide and the mitochondrial respiratory chain. Biochimie *100*, 88–94. https://doi.org/10.1016/j.biochi.2013.07.027.

Labusch, M., Mancini, L., Morizet, D., and Bally-Cuif, L. (2020). Conserved and Divergent Features of Adult Neurogenesis in Zebrafish. Front. Cell Dev. Biol. *8*, 525. https://doi.org/10.3389/fcell.2020.00525.

Leeman, D.S., Hebestreit, K., Ruetz, T., Webb, A.E., McKay, A., Pollina, E.A., Dulken, B.W., Zhao, X., Yeo, R.W., Ho, T.T., et al. (2018). Lysosome activation clears aggregates and enhances quiescent neural stem cell activation during aging. Science *359*, 1277–1283. https://doi.org/10.1126/science.aag3048.

Lefrancois, S., Zeng, J., Hassan, A.J., Canuel, M., and Morales, C.R. (2003). The lysosomal trafficking of sphingolipid activator proteins (SAPs) is mediated by sortilin. EMBO J. *22*, 6430–6437. https://doi.org/10.1093/emboj/cdg629.

Liang, R., Arif, T., Kalmykova, S., Kasianov, A., Lin, M., Menon, V., Qiu, J., Bernitz, J.M., Moore, K., Lin, F., et al. (2020). Restraining Lysosomal Activity Preserves Hematopoietic Stem Cell Quiescence and Potency. Cell Stem Cell *26*, 359–376.e7. https://doi.org/10.1016/j.stem.2020.01.013.

Llorens-Bobadilla, E., Zhao, S., Baser, A., Saiz-Castro, G., Zwadlo, K., and Martin-Villalba, A. (2015). Single-Cell Transcriptomics Reveals a Population of Dormant Neural Stem Cells that Become Activated upon Brain Injury. Cell Stem Cell *17*, 329–340. https://doi.org/10.1016/j.stem.2015.07.002.

Mancini, L., Guirao, B., Ortica, S., Labusch, M., Cheysson, F., Bonnet, V., Phan, M.S., Herbert, S., Mahou, P., Menant, E., et al. (2023). Apical Size and deltaA Expression Predict Adult Neural Stem Cell Decisions along Lineage Progression. Sci Adv. *9*, eadg7519. https://doi.org/10.1101/2022.12.26.521937.

Marcy, G., Foucault, L., Babina, E., Capeliez, T., Texeraud, E., Zweifel, S., Heinrich, C., Hernandez-Vargas, H., Parras, C., Jabaudon, D., and Raineteau, O. (2023). Single-cell analysis of the postnatal dorsal V-SVZ reveals a role for Bmpr1a signaling in silencing pallial germinal activity. Sci. Adv. *9*, eabq7553. https://doi.org/10.1126/sciadv.abq7553.

März, M., Chapouton, P., Diotel, N., Vaillant, C., Hesl, B., Takamiya, M., Lam, C.S., Kah, O., Bally-Cuif, L., and Strähle, U. (2010). Heterogeneity in progenitor cell subtypes in the ventricular zone of the zebrafish adult telencephalon. Glia *58*, 870–888. https://doi.org/10.1002/glia.20971.

Meyer, R.C., Giddens, M.M., Coleman, B.M., and Hall, R.A. (2014). The Protective Role of Prosaposin and Its Receptors in the Nervous System. Brain Res. *1585*, 1–12. https://doi.org/10.1016/j.brainres.2014.08.022.

Mizrak, D., Levitin, H.M., Delgado, A.C., Crotet, V., Yuan, J., Chaker, Z., Silva-Vargas, V., Sims, P.A., and Doetsch, F. (2019). Single-Cell Analysis of Regional Differences in Adult V-SVZ Neural Stem Cell Lineages. Cell Rep. *26*, 394–406.e5. https://doi.org/10.1016/j.celrep.2018.12.044.

Mony, V.K., Benjamin, S., and O'Rourke, E.J. (2016). A lysosome-centered view of nutrient homeostasis. Autophagy *12*, 619–631. https://doi.org/10.1080/15548627.2016.1147671.

Morizet, D., Foucher, I., Alunni, A., and Bally-Cuif, L. (2023). Integrative Single-Cell Transcriptomics Clarifies Adult Neurogenesis and Macroglia Evolution. Preprint at bioRxiv. https://doi.org/10.1101/2023.02.27.530203.

Paik, J.h., Ding, Z., Narurkar, R., Ramkissoon, S., Muller, F., Kamoun, W.S., Chae, S.-S., Zheng, H., Ying, H., Mahoney, J., et al. (2009). FoxOs cooperatively regulate diverse pathways governing neural stem cell homeostasis. Cell Stem Cell *5*, 540–553. https://doi.org/10.1016/j.stem.2009.09.013.

Pilz, G.-A., Bottes, S., Betizeau, M., Jörg, D.J., Carta, S., April, S., Simons, B.D., Helmchen, F., and Jessberger, S. (2018). Live imaging of neurogenesis in the adult mouse hippocampus. Science *359*, 658–662. https://doi.org/10.1126/science.aao5056.

Schäffner, I., Minakaki, G., Khan, M.A., Balta, E.-A., Schlötzer-Schrehardt, U., Schwarz, T.J., Beckervordersandforth, R., Winner, B., Webb, A.E., DePinho, R.A., et al. (2018). FoxO Function Is Essential for Maintenance of Autophagic Flux and Neuronal Morphogenesis in Adult Neurogenesis. Neuron *99*, 1188–1203.e6. https://doi.org/10.1016/j.neuron.2018.08.017.

Shin, J., Berg, D.A., Zhu, Y., Shin, J.Y., Song, J., Bonaguidi, M.A., Enikolopov, G., Nauen, D.W., Christian, K.M., Ming, G.l., and Song, H. (2015). Single-Cell RNA-Seq with Waterfall Reveals Molecular Cascades underlying Adult Neurogenesis. Cell Stem Cell *17*, 360–372. https://doi.org/10.1016/j.stem.2015.07.013.

Than-Trong, E., Kiani, B., Dray, N., Ortica, S., Simons, B., Rulands, S., Alunni, A., and Bally-Cuif, L. (2020). Lineage hierarchies and stochasticity ensure the long-term maintenance of adult neural stem cells. Sci. Adv. *6*, eaaz5424. https://doi.org/10.1126/sciadv.aaz5424.

Urbán, N., van den Berg, D.L.C., Forget, A., Andersen, J., Demmers, J.A.A., Hunt, C., Ayrault, O., and Guillemot, F. (2016). Return to quiescence of mouse neural stem cells by degradation of a proactivation protein. Science *353*, 292–295. https://doi.org/10.1126/science.aaf4802.

Urbán, N., Blomfield, I.M., and Guillemot, F. (2019). Quiescence of Adult Mammalian Neural Stem Cells: A Highly Regulated Rest. Neuron *104*, 834–848. https://doi.org/10.1016/j.neuron.2019.09.026.

Zeng, J., Racicott, J., and Morales, C.R. (2009). The inactivation of the sortilin gene leads to a partial disruption of prosaposin trafficking to the lysosomes. Exp. Cell Res. *315*, 3112–3124. https://doi.org/10.1016/j.yexcr.2009.08.016.

Zhao, X.-F., Fjose, A., Larsen, N., Helvik, J.V., and Drivenes, Ø. (2008). Treatment with small interfering RNA affects the microRNA pathway and causes unspecific defects in zebrafish embryos. FEBS J. *275*, 2177–2184. https://doi.org/10.1111/j.1742-4658.2008.06371.x.

Zhou, X., Sullivan, P.M., Sun, L., and Hu, F. (2017). The interaction between progranulin and prosaposin is mediated by granulins and the linker region between saposin B and C. J. Neurochem. *143*, 236–243. https://doi.org/10.1111/jnc.14110.

Zweifel, S., Marcy, G., Lo Guidice, Q., Li, D., Heinrich, C., Azim, K., and Raineteau, O. (2018). HOPX Defines Heterogeneity of Postnatal Subventricular Zone Neural Stem Cells. Stem Cell Rep. *11*, 770–783. https://doi.org/10.1016/j.stemcr.2018.08.006.